PCCP

CrossMark
click for updates

Critical assessment of enhancement factor measurements in surface-enhanced Raman scattering on different substrates†

Daniel C. Rodrigues,[a] Michele L. de Souza,[a] Klester S. Souza,[a] Diego P. dos Santos,[b] Gustavo F. S. Andrade[c] and Marcia L. A. Temperini*[a]

The SERS enhancement factor (SERS-EF) is one of the most important parameters that characterizes the ability of a given substrate to enhance the Raman signal for SERS applications. The comparison of SERS intensities and SERS-EF values across different substrates is a common practice to unravel the performance of a given substrate. In this study, it is shown that such a comparison may lack significance if we compare substrates of very distinct nature and optical properties. It is specifically shown that the SERS-EF values for static substrates (*e.g.* immobilized metallic nanostructures) cannot be compared to those of dynamic ones (*e.g.* colloidal metal nanoparticle solutions), and that the optical properties for the latter show strong dependence on the metal–molecule interaction dynamics. The most representative experimental results concerning the dynamic substrates have been supported by generalized Mie theory simulations, which are tools used to describe the substrate complexity and the microscopic information not usually taken into account.

[a] *Laboratório de Espectroscopia Molecular, Instituto de Química,*
  Universidade de São Paulo, C.P. 26077, CEP 05513-970, São Paulo, Brazil.
  E-mail: mlatempe@iq.usp.br
[b] *Departamento de Físico-Química, Instituto de Química,*
  Universidade Estadual de Campinas, CP 6154, CEP 13083-970, Campinas, Brazil
[c] *Laboratório de Nanoestruturas Plasmônicas, Núcleo de Espectroscopia e Estrutura*
  Molecular (NEEM), Departamento de Química, Universidade Federal de Juiz de
  Fora, Juiz de Fora, Brazil
† Electronic supplementary information (ESI) available: Determination of roughness factor, SERS in nmol L^{-1}, Monte Carlo simulations, additional SEM images of AuNS in the presence of KCl/4MPy. See DOI: 10.1039/c4cp05080k

1. Introduction

The discussion on the enhancement of the effective cross-section Raman scattering observed in the SERS effect has been a source for several arguments over the literature[1–4] which have resulted in a long series of works with several different procedures for the Raman Scattering Enhancement quantification, the so-called SERS enhancement factor (SERS-EF). Le Ru and Etchegoin have formulated a very important discussion on the different methods to calculate the SERS-EF.[5] The reported methods in that work can be used in several complexity levels, varying from simple calculations of the change in Raman intensity in the presence of nanostructures to procedures that take into account the available area of plasmonic nanoparticles and the effective number of adsorbed molecules that contribute to the SERS-EF.

The SERS-EF has been used by several research groups in order to characterize the performance of the SERS substrates.[6] The development of new substrates results in the need to compare them to others already presented in the literature. The SERS-EF evaluation is considered a powerful tool for inter-experimental comparisons. It is noticeable, however, that the SERS substrates have been prepared in several different ways as nanolithographic structures,[7–9] nanostructures immobilized on solid supports,[10] solid electrodes[11] and nanoparticles in suspension.[12,13] Some of these substrates reach the necessary conditions to work in a single-molecule SERS regime.[14–17] One can easily notice that the new substrate research is a relevant topic in SERS because it paves the way to platforms where the responsive signal is spatially huge and homogeneous. This ultimately turns the SERS into a routine technique to detect and characterize adsorbates such as drugs, dyes, conducting polymers, agrochemicals, and cancer related proteins, among others present in sub-trace levels. Many SERS research communities have made great efforts to work under this condition.[18–25]

It is important to notice that in the literature, there are different methodologies leading to a wide range of SERS-EFs with the same experimental results and a large range of values for various types of substrates. The reported SERS-EF values have spanned from 10^3 to 10^{14}. Nonetheless, such deviation not only reflects the variety of SERS substrates but also points to the need for systematization in the experimental measurement of the SERS-EF and its correct application.

21294 | *Phys. Chem. Chem. Phys.,* 2015, **17**, 21294–21301

This journal is © the Owner Societies 2015

In the present work, the SERS-EFs for several substrates are presented such as roughened electrodes (AuEle), fixed Au nanotubes (AuNT), Klarite® and spherical nanoparticle suspensions (AuNS). Also in discussion is the application viability of the SERS-EF measurement for a wide range of SERS substrates as a relative performance criterion. It is shown that it is not recommended to use the SERS-EF to directly compare static substrates like AuEle and AuNT, *i.e.* immobilized metallic nanostructures, to dynamic ones (colloidal AuNS) whose optical properties and therefore SERS performances depend on the nanoparticle interaction dynamics sensitive to a particular set of experimental conditions. The experimental results for the dynamic substrates have been simulated using generalized Mie theory calculations as a tool to obtain a microscopic view of the systems.

2. Experimental section

2.1. Chemicals

Purification of 4-mercaptopyridine (4MPy, 95%, Sigma-Aldrich) was performed by recrystallization from ethanol (95%, Nuclear, Brazil), and the SERS experiments used freshly recrystallized 4MPy in order to avoid probe-molecule degradation. All aqueous solutions were prepared employing deionized water (18.2 MΩ cm). KCl (99.5%, Merck), $HAuCl_4$ (99.9%, Plat-Lab, Brazil), sodium citrate dihydrate (99+%, Sigma-Aldrich) and dichloromethane (99.5%, Synth, Brazil) were used without further purification.

Porous polycarbonate membranes (PCM, Sterlich) with nominal pore diameters (Φ) of 50, 100, 200 and 400 nm were purchased from Sterlitech Corporation. Gold target (99.9%) was purchased from Plat-Lab, Brazil. The electrochemical system consists of a 0.4 cm diameter gold electrode (99.99%, Plat-Lab, Brazil) as the working electrode inserted in a Teflon® matrix, a platinum wire (0.50 mm diameter, 100%, Plat-Lab, Brazil) as the counter-electrode and Ag(s)|AgCl(s)|KCl(sat) as the reference electrode. Klarite® substrate was used as received.

2.2. Equipment

Scanning electron microscopy images were obtained on a JEOL JSM-7401 F-Field Emission Scanning Electron Microscope and a JEOL NeoScope JCM-5000. The Au sputtering system consisted of an Edwards Scancoat Six and a quartz microbalance Edwards FTM6. The electrochemical roughening of the Au electrode was performed on an AUTOLAB PGSTAT101 potentiostat/galvanostat.

The SERS and Raman experiments were performed in a Renishaw InVia Reflex coupled to a Leica DM2500M microscope, with the He–Ne excitation laser line at 633 nm, diode laser with emission at 785 nm and water immersion objective lens with 63× magnification, NA = 0.9. For 633 nm, the confocal area was measured as 1.0 μm² (A_{conf}) and the confocal volume of 14.6 μm³ (V_{conf}) was used according to a method proposed in the literature.[26]

2.3. SERS substrate preparation and spectra acquisition

Au nanospheres (AuNS) were synthesized employing a methodology proposed by Frens,[27] and they had a LSPR band maximum at 528 nm, a diameter of 45 ± 5 nm and a concentration of 3.4×10^{12} AuNS cm⁻³.[28] For the SERS experiments, a desired concentration of the probe solution (10×10^{-3}, 1.0×10^{-3} or 0.1×10^{-3} mol L⁻¹ for regular SERS-EF comparison, and 20×10^{-9}, 40×10^{-9} or 60×10^{-9} mol L⁻¹ for investigation in low concentrations), and the aggregation agent (KCl solution to final concentration of 1.0×10^{-3} mol L⁻¹) was added to the AuNS suspension. For the SERS-EF measurements, 350 spectra were sequentially obtained for each concentration after 5 min of sample preparation. For the investigation in low concentration, 100 spectra were averaged. The laser power at the sample was constant at 8.0×10^4 W cm⁻².

Au electrode (AuEle) cleaning was performed through immersion in a $KMnO_4$ solution for 1 h, followed by rinsing with deionized water, immersion in piranha solution for 10 min, and then washing thoroughly with deionized water. After the cleaning procedure, the AuEle was mechanically polished and washed abundantly with deionized water. The SERS activation of the electrode consisted of oxidation–reduction cycles (ORCs) performed in 0.1 mol L⁻¹ KCl aqueous solution: 2 cycles in the −1.20 V to +1.15 V range and 20 cycles in the −0.20 V to +1.15 V range, both at a scan rate of 100 mV s⁻¹ (Fig. S1A, ESI†).[26,29,30]

The active surface area for the AuEle was determined through cyclic voltammetry in the range from −0.3 V to +1.5 V, starting from 0 V at a scan rate of 100 mV s⁻¹ in 0.5 mol L⁻¹ H_2SO_4(aq) solution (Fig. S1B, ESI†), following the procedure of Trasatti and Petrii.[31] The roughening factor obtained was R = 1.83 (see details of the measurement of R in the ESI†).

After the ORCs, the electrode was thoroughly rinsed with deionized water and immersed in a 0.1×10^{-3} mol L⁻¹ 4MPy solution for 5 min. The surface modified electrode was abundantly washed with deionized water and kept immersed in deionized water during SERS spectra acquisition.

The procedure for obtaining Au nanotubes (AuNT) built on thin-Au films employing the polycarbonate track-etched membrane (PCM) method has been reported previously.[9] Briefly, a 100 nm Au film was sputtered on one side of a PCM with the desired pore size, with plasma pressure of *ca.* 0.2 mbar and two different applied potentials: 0.75 (initial 5 nm deposition) and 1.25 kV (for deposition up to 100 nm). After Au sputtering, the gold coated side of the membrane was immobilized on a copper tape. The PCM template was then removed by successive exposure to CH_2Cl_2 (Synth, Brazil); the final films presented a greenish coloration. The AuNT and Klarite® substrates underwent the same 4MPy adsorption procedure as described for AuEle.

The SERS-EFs for the static substrates were calculated based on an average over several spectra obtained in the SERS mapping of each substrate: 121 spectra for the AuNT, 120 spectra for AuEle and 440 spectra for Klarite®.

2.4. Computational simulations

Generalized Mie theory. The plasmonic properties of gold nanospheres (AuNS substrate) were simulated in the formalism of the generalized Mie theory (GMT), by using the GMM-field code.[32–35] In such simulations, the experimental values for the

This journal is © the Owner Societies 2015

Phys. Chem. Chem. Phys., 2015, **17**, 21294–21301 | **21295**

dielectric function of Au obtained from the Johnson and Christy compilation have been used.[36]

3. Results and discussion

3.1. SERS spectra

Fig. 1 shows the SERS spectra of 4MPy adsorbed on different SERS substrates (AuEle, AuNS, Klarite® and AuNT) in comparison to the normal Raman spectrum of 4MPy in aqueous solution. Additional SEM images of AuNT may be found in the ESI† (Fig. S2). For each experiment, the only parameter that has been changed is the nanostructure shape of all substrates, which is responsible for the Raman signal enhancement. The changes in the SERS spectra and enhancement factors when comparing different substrates are directly related to the changes in surface plasmon resonance conditions, which are dependent on the shape of the nanostructures. Therefore, in Fig. 1, a SEM image for each substrate depicts the characteristic morphological properties for the investigated nanostructures.

All SERS spectra in Fig. 1 show changes in relative intensities and observed frequencies relative to the normal Raman spectrum of 4MPy, which is expected due to molecule chemical adsorption on Au surfaces. The 4MPy adsorption on the Au surface has caused a shift of the band ($\nu_{CC,trigonal}/\nu_{C=S}$) from 1114 cm^{-1} in the normal Raman spectrum to *ca.* 1090 cm^{-1} in all SERS spectra.

Of all SERS spectra, the 4MPy spectrum on the AuNS substrate is the one that most resembles a normal Raman spectrum. Nevertheless, it presents a slightly smaller relative intensity between the bands at *ca.* 1000 cm^{-1} ($\nu_{CC,ring\ breathing}$) and 1200 cm^{-1} (β_{CH}/δ_{NH}) than the ones observed in normal

Fig. 1 Average SERS spectra of 4-MPy 1×10^{-2} mol L^{-1} in different Au substrates and their respective SEM images. Raman spectrum of the bulk 4MPy is present at the bottom of the figure. $\lambda_0 = 633$ nm.

Raman conditions. This behavior is due to the plasmon coupling field profile, which originated from the aggregation of AuNS. This subject will be discussed later in this paper.

On the other hand, the SERS spectra for immobilized metallic nanostructures such as AuEle, Klarite® and AuNT presented very similar relative intensities. There is a small difference in the SERS spectra for AuNT. The ring breathing mode has been observed at *ca.* 1016 cm^{-1} in contrast to at 1000 cm^{-1} for the other two substrates. This variation was previously attributed to different adsorption geometries.[9,11,37]

Therefore, in order to compare the different abilities of the substrates to enhance the Raman signal, the EF values have been calculated using a band at *ca.* 1090 cm^{-1}, which presents the smallest change in relative intensity among the substrates. In the next section, the calculated EF for each substrate will be presented, taking into account the results obtained in Fig. 1.

3.2. SERS-EF and related quantities

Eqn (1) below was used to calculate the EF[26]

$$\text{EF} = \frac{I_{SERS}/N_{SERS}}{I_{bulk}/N_{bulk}} \qquad (1)$$

where I_{SERS} and I_{bulk} are the intensities of the given SERS and Raman bands, respectively, and N_{SERS} and N_{bulk} stand for the number of scatterers in the SERS and Raman spectral acquisitions, respectively. N_{bulk} has been determined in the same experimental conditions as those used for the SERS experiments, except for the absence of a metallic surface, and its value solely depends on the concentration of solution and the objective confocal volume (V_{conf}). Differently, N_{SERS} is related to the number of probe molecules adsorbed on the metallic substrate, and it is obtained considering the SERS-active surface coverage (Γ) on the objective confocal area (A_{conf}) for static substrates, or on the confocal volume (V_{conf}) for dynamic ones.

Regarding the EF values for distinct substrates, special attention has been paid to the difference between their morphologies in order to have the proper correction factor for N_{SERS}, aiming to solely consider the molecules that effectively contribute to the SERS enhancement.

For the AuNS system, which is the dynamic substrate in this study, N_{SERS} in eqn (1) has been obtained considering previous works where the concentration limit for the adsorption of a 4MPy monolayer on a flat Au surface coverage at 1.0×10^{-3} mol L^{-1} has resulted in $\Gamma = 4.7 \times 10^{-10}$ mol cm^{-2}.[38,39] Taking into account the concentration of AuNS (3.4×10^{12} AuNS cm^{-3} or 5.6×10^{-9} mol AuNS L^{-1}), the V_{conf} (14.6 μm^3) and the average diameter of the AuNS (45 ± 5 nm), the total available surface area of the AuNS has been estimated to be 2.86×10^{-9} cm^2 inside V_{conf}.[26] The N_{SERS} for 4MPy adsorbed in the first monolayer on the AuNS is 8.97×10^{-5} mol L^{-1}, and therefore, in this study, there has been an excess of 4-MPy in the solution, assuring the complete surface coverage of the AuNS. In fact, the average SERS-EF of 4-MPy on AuNS has similar values for different concentrations (Fig. S3A and Table S1, ESI†).

For static substrates, a correction factor for the A_{conf} should be considered, because the SERS active surfaces are not flat.
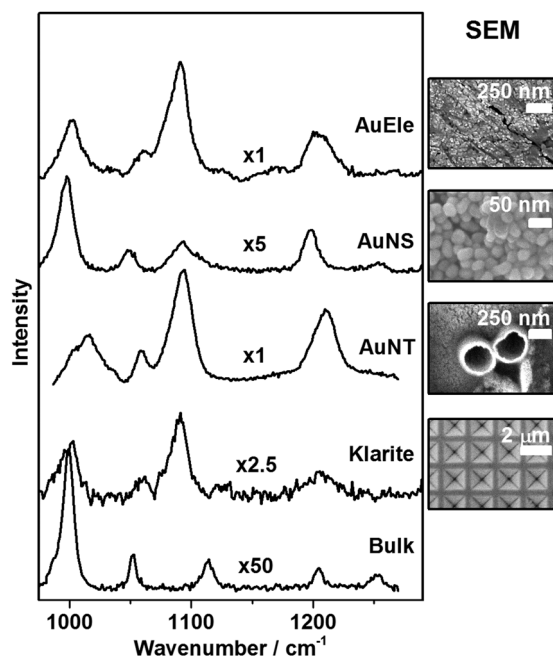
21296 | *Phys. Chem. Chem. Phys.,* 2015, **17**, 21294–21301

This journal is © the Owner Societies 2015

The correction factor must take into account an effective illuminated area during the SERS experiment due to the different topography of the substrates under the laser spot. For instance, the surface area of the AuEle after the ORC procedure resulted in a roughness factor (R) of 1.8, which means that the activated AuEle presents a real area 180% larger than a flat electrode.

Besides the morphology of the AuNT, the substrate non-uniformity, due to the disorganized build-up of the template, has been corrected considering the density of AuNT (d_{AuNT}) in the A_{conf}. Based on several SEM images over the surface of the AuNT substrates, d_{AuNT} has been estimated to be 6, 4, 1.5 and 0.7 μm^{-2} for PCMs with diameters (Φ) of 50, 100, 200 and 400 nm, respectively. The N_{SERS} has been obtained by the product of the number of scatterers under the laser spot ($A_{conf} \times \Gamma$) corrected by the number of SERS enhancing structures ($A_{conf} \times d_{AuNT}$). Distinctively, the Klarite® substrate presents high morphological homogeneity over a large area with pyramidal indents, which are the SERS-active spots for the substrate. Its estimated microstructure density (d_{MS}) is 2.5 μm^{-2} when several SEM images are obtained. The SERS spectra obtained as a function for the focus depth (1.5 μm deep into the focused beam) have presented subtle differences on the SERS performance and consequently on the SERS-EF. This has occurred because the change in height throughout the measurement is smaller than the confocal height (H_{conf} = 14.6 μm); therefore, only the spectra obtained under a focused beam have been considered to calculate the SERS-EF.

Based on the SERS spectra shown in Fig. 1, Table 1 presents the SERS-EF values as well as the corresponding standard deviations for 4MPy adsorbed on each substrate. In order to analyze such data, the relative SERS performance of the AuNT substrates will be discussed (in terms of EF values and their spatial dispersion) with respect to the substrates whose performances have been extensively studied, such as AuEle and AuNS, which present strong enhancing characteristics and are capable of single-molecule detection (especially AuNS), and Klarite®, a substrate with high reproducibility for SERS intensity characteristics.

The data in Table 1 indicate that the greatest SERS-EF has been obtained for AuNT (Φ = 400 nm) in comparison to the other substrates, whose values are extremely higher if compared to the dynamic substrate (AuNS). A very important result from Table 1 relies on the EF dispersion. The values obtained for the standard deviation for AuNT substrates are less than

50% of the average SERS-EF, which is similar to the experimental situation observed for Klarite®.

The highest SERS-EF for AuNT among the presented substrates is actually expected considering the existence of a large number of hot-spots on the mapped area (such as the ones formed by the coalesced 400 nm AuNT shown in the SEM image in Fig. 1). On the other hand, Klarite® is an organized substrate with no strong hot-spots in the SERS mapped area, which leads to a significantly smaller SERS enhancement. The AuEle is a highly disorganized substrate with a wide range of structures, some with LSPR at the laser wavelength, which contribute to high SERS-EF values, and others very far from it, which contribute to very low EF values. This broad range of LSPR resonances is the most probable origin for the observed high values of standard deviation in the SERS-EF in Table 1.

Although, apparently, it has been possible to justify the EF values, intriguing data have been obtained, specifically the very low EF value of AuNS. It can be noticed that in the comparison among substrates, a fundamental point has not been taken into account: the resonance between the excitation radiation and the LSPR. The comparison of substrates is not considered "fair", because they present very distinct optical properties, for instance, in terms of the LSPR resonance position. In order to emphasize this point, the extinction spectra of AuNT and AuNS will be discussed. For instance, Fig. 2 presents the Kubelka–Munk spectra for the AuNT substrates for different values of Φ.

The extinction band in Fig. 2 near 500 nm observed in all AuNT samples has a great absorption contribution due to the rough gold film on which they are grown in addition to the LSPR of the AuNT. Therefore, the discussion will rely solely on the bands at longer wavelengths, which correspond to the localized surface plasmon resonance for the AuNT on the samples. For pore diameters Φ = 200 nm and 400 nm, the samples present plasmon resonance very close to the laser excitation wavelength in the SERS experiments (633 nm), especially for Φ = 400 nm. Therefore, such a substrate, whose optical properties are in resonance with the incident laser, should present better enhancement properties as indeed observed experimentally in Table 1.

3.3. AuNS LSPR behavior towards 4MPy aggregation

The most surprising result is the very small SERS-EF value measured for the AuNS substrate. It is well known that such a substrate is capable of single-molecule SERS detection,[40,41] which does not seem to be in agreement with the SERS-EF results.

Since we are comparing the performances of different SERS substrates, common sense would be to keep the same experimental conditions in terms of the probe molecule and instrumental setup conditions. Such an approach has resulted in a very small SERS-EF for the AuNS substrate. Fig. 3 shows the extinction spectra for the AuNS colloid before and after the addition of KCl (which promotes aggregation) and 4MPy. One can clearly see that the AuNS aggregate in such a way that a new plasmon resonance band appears in the extinction spectrum

Table 1 SERS-EF values for 1.0×10^{-2} mol L^{-1} 4MPy on gold substrates on the basis of the $\nu_{CC,trigonal}/\nu_{C=S}$ vibrational band at 1090 cm^{-1}

SERS substrate	EF $\pm$ σ/10^3
AuEle	39 $\pm$ 73
AuNS[a]	1.4 $\pm$ 0.14
AuNT Φ 50 nm	5.8 $\pm$ 0.8
AuNT Φ 100 nm	7.8 $\pm$ 3.0
AuNT Φ 200 nm	20 $\pm$ 11
AuNT Φ 400 nm	120 $\pm$ 50
Klarite	4.2 $\pm$ 2.0

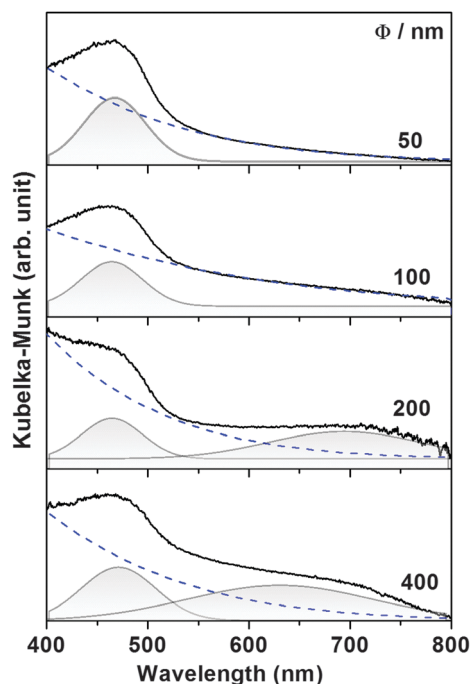[a] AuNS EF value on the basis of the band at 1000 cm^{-1}.

Fig. 2 Kubelka–Munk spectra of the substrates generated by gold deposition by sputtering inside the PCM pores of different diameters (Φ), deconvoluted extinction bands in light grey lines and Au interband transition in blue dashed lines. (Adapted from ref. 9)
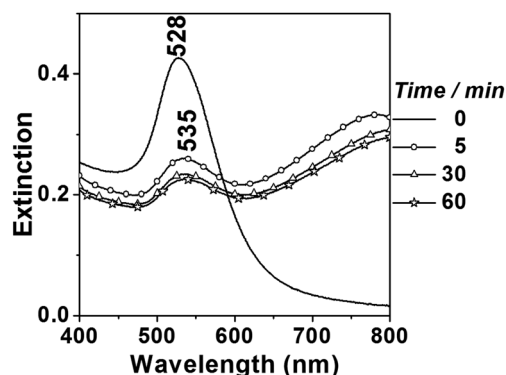

Fig. 3 Extinction spectra of AuNS before (solid line) and after (different times) addition of 1.0×10^{-2} mol L^{-1} 4MPy and KCl 1.0×10^{-3} mol L^{-1}.

close to 800 nm. Note that 5 min after addition of KCl and 4MPy, the extinction spectrum maintains approximately the same shape. The very same behavior has been observed for 1.0×10^{-3} mol L^{-1} and 1.0×10^{-4} mol L^{-1} (Fig. S3B, ESI†). This is the reason for the low EF values obtained by this substrate under an excitation wavelength at 633 nm, which emphasizes that the comparison of SERS-EF between AuNT and AuNS is somewhat meaningless for such experimental conditions, because the plasmon resonances for AuNS are very far from the laser excitation wavelength.

Additional experimental conditions have been investigated in low concentrations of 4MPy as a strategy aiming at a better understanding of the SERS enhancement in the AuNS substrate. It is well known that the formation of clusters of AuNS in
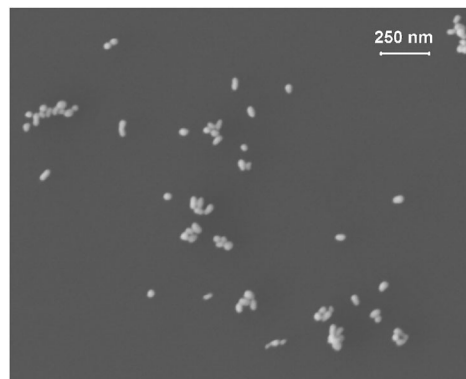

Fig. 4 SEM image for the AuNS substrate after aggregation with 4MPy (60 nmol L^{-1}). The nanostructures have been deposited on a silicon wafer for image acquisition.

suspension depends on the KCl concentration as well as the concentration of 4MPy,[42] which adsorbs on the AuNS surface, displacing the stabilizing citrate layer and changing the particle surface charge. In that sense, the formed AuNS clusters may present a redshift or a new band in the LSPR spectra, which can result in the plasmon resonance being very far from the laser excitation wavelength. To study that behavior, SEM experiments have been performed on AuNS aggregated with KCl and 4MPy in nanomolar concentrations (SEM images of 60 nmol L^{-1} in Fig. 4 and in concentration range from 20 to 60 nmol L^{-1} in Fig. S4–S6, ESI†). Simulations have also been made by the GMT for different aggregates of AuNS, as presented in Fig. 5 for linear arrays of nanostructures separated by a gap distance of 1 nm.

A linear array is the chosen model for studying the aggregation dynamics of colloidal solutions. If the nanoparticles still have surface charges, there is a large probability of forming approximately linear aggregates to diminish electrostatic repulsions, as can be observed by the Monte Carlo simulations based on DLVO theory, which are presented as supporting information (see the ESI†). Therefore, even though the model does not exactly match the experimental SEM, it is still a good approximation to describe the optical properties of small and large clusters in such a system.

In Fig. 5, one can see that the dipolar coupling surface plasmon resonance wavelength redshifts as the number of AuNS increases in the aggregate, as expected. For small AuNS aggregates, it is possible to observe plasmon resonances closer to the laser excitation (633 nm) as in the case of dimers, for instance. However, the maximum wavelength for such a plasmon resonance approaches an asymptotic limit of 800 nm in aggregates with a large number of particles. This maximum value is approximately the same as that observed experimentally for LSPR of AuNS in the presence of 4MPy and KCl in Fig. 3, and hence, the linear array of particles separated by gap distance of 1 nm is a good approximation to describe the experimental results.

A proper comparison between AuNT and AuNS substrates happens for the latter and is constituted mostly by dimers, a condition that is not easy to achieve experimentally and which
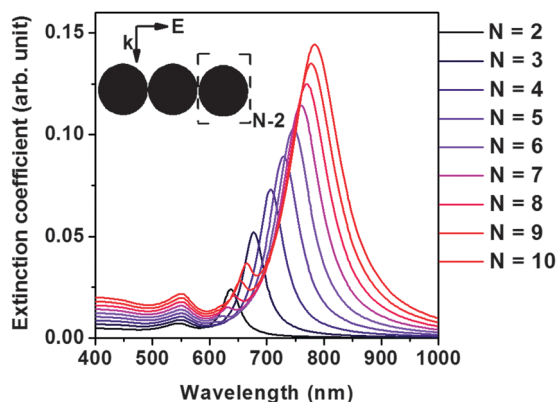
Fig. 5 Simulated extinction spectra for different numbers of AuNS in a linear array.

is far from the experimental observations in Fig. 3 and 4. However, the experimental conditions for 4MPy concentration can be tuned in such a way to result in a higher probability of having dimers than the other aggregates. Keeping that in mind, experiments with much lower 4MPy concentrations (20, 40 and 60 nmol L^{-1}) have been performed. Such concentrations are on the same order of magnitude as the concentration of AuNS present in the colloidal solution (56 nmol L^{-1} AuNS). The extinction spectra and SERS for the mixture AuNS + 4MPy + KCl (1.0×10^{-3} mol L^{-1}) as a function of 4MPy concentration are presented in Fig. 6.

It can be observed in Fig. 6A that along with the 532 nm LSPR band, there is an emerging band at a larger wavelength as the 4MPy concentration increases. These bands are assigned to single and aggregated nanoparticles, respectively. The change in the LSPR spectra of AuNS with the addition of 4MPy has led to higher SERS intensities at 785 nm (Fig. 6B).

The LSPR spectrum for the system 4MPy (20 nmol L^{-1}) + AuNS (Fig. 6A) does not present an additional band other than the maximum extinction of the AuNS at 532 nm, which does not present any shifting, suggestin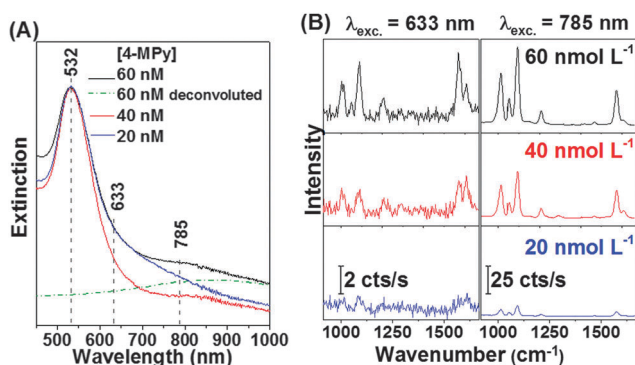g that most of the particles are not aggregated (Fig. S4, ESI†). At such a low concentration, small aggregated AuNS may be formed but the extinction spectrum does not have enough sensitivity to display the changes. A new extinction band arises above 800 nm as the concentration of 4MPy increases to 40 nmol L^{-1} due to the more evident formation of aggregated AuNS (as can be seen in Fig. S5, ESI†), which increases even more for 60 nmol L^{-1} of 4MPy (Fig. S6, ESI† and Fig. 4). It is worth mentioning that even at such low concentrations, the extinction bands have not increased in the region around 633 nm.

Thus, the SERS spectra excited at 633 nm (Fig. 6B), as expected, have presented a low magnification of the Raman signal of 4MPy adsorbed on disperse AuNS, whereas the 785 nm excitation presented a much larger SERS enhancement, even for a 4MPy concentration of 20 nmol L^{-1}. This suggests that upon 4MPy addition to the colloidal solution, the local concentration of the probe molecule can be higher than the expected final concentration,[43] a situation that leads to a higher degree of exchange between 4MPy and citrate on the nanosphere surface, facilitating the aggregation of the nanospheres, whose evolution is easily verified in the SEM micrographs in Fig. S4–S6 (see ESI†).

This interpretation can be further reinforced by the shape of the SERS spectra under excitation at 633 and 785 nm laser wavelengths. For 633 nm excitation, in comparison to 785 nm, it is possible to observe SERS spectra with higher relative intensities for the bands at *ca.* 1600 cm^{-1} with respect to the bands at *ca.* 1000 cm^{-1}. This result suggests an influence of the local field enhancement factor resonance position on the relative intensities on the SERS spectra.

For the sake of reinforcing the interpretation above, Fig. 7 presents the results of GMT simulation for a given set of aggregates obtained in a Monte Carlo simulation of AuNS in the presence of ions (see ESI†) for two wavelength excitations, 633 nm (Fig. 7A) and 785 nm (Fig. 7B).

The local field enhancement factor (EF) maps in Fig. 7 show that small aggregates (such as dimers and trimers) make a greater contribution to field enhancement for excitation at 633 nm than at 785 nm. It is also possible to observe that for some large aggregates (such as the ones with 12 spheres in the simulations), some regions of the structure (marked by a white dashed ellipse in Fig. 7A) may present a higher contribution to the SERS signal for 633 nm than for 785 nm. Therefore, even though the experimental extinction band spectrum has not shown any maximum extinction at such a wavelength in Fig. 6A, the increase in the 4MPy concentration leads to the formation of clusters that may present strong local field enhancements at 633 nm, hence contributing to an increase in the SERS intensity for such a wavelength, as observed in Fig. 6B. This result further highlights the complexity of the comparison of SERS-EF for a fixed substrate and a dynamic substrate like AuNS, for which there may exist a much broader distribution of local field enhancement resonances.

In Fig. 7C, there is the EF profile values in the SERS spectrum range for the hot spot marked as (i) and (ii) in Fig. 7A and B, respectively. The EF profile for 785 nm shows a

Fig. 6 (A) Extinction spectra of AuNS suspension in comparable concentrations of 4MPy (green dashed line: curve-fit for a band representing AuNS aggregates, vertical dashed lines represent the maximum extinction at 532 nm for monomeric AuNS and the SERS laser wavelengths at 633 and 785 nm); (B) SERS spectra of 4MPy in AuNS suspension under 633 nm and 785 nm excitation lasers.

This journal is © the Owner Societies 2015

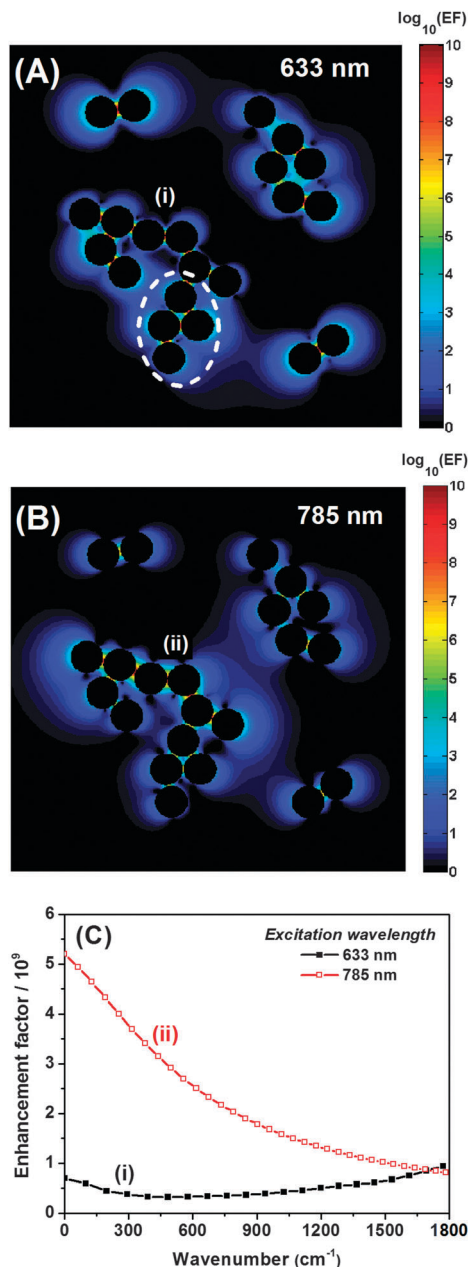*Phys. Chem. Chem. Phys.*, 2015, **17**, 21294–21301 | **21299**

Fig. 7 Local electric field enhancement factor map simulations for 633 nm (A) and 785 nm (B) for a set of aggregates observed in Monte Carlo simulations. The enhancement factors have been calculated by the product of the square of the local field enhancement at two wavelengths: incident wavelength and a wavelength shifted by 1000 cm^{-1} from the incident. (C) EF profiles for wavelengths shifted from the incident wavelength in the range 0 to 1800 cm^{-1} for the points marked (i) and (ii) in (A) and (B). The black and red curves correspond to the EF profile for incident wavelengths at 633 nm and 785 nm, respectively.

much larger enhancement in the low frequency range, whereas for 633 nm, the observed enhancements are higher for the high frequency region of the SERS spectrum, which is in accordance with the ones observed in Fig. 6B. It should be noticed that this model has not aimed to simulate the exact experimental conditions but rather to draw attention to the fact that the SERS intensities and therefore the EF values depend upon the local field properties of the nanostructures as well as on the local field distribution on each particle. For AuNS, a dynamic substrate, this local field distribution may be very complex and show strong dependence on the experimental conditions.

4. Conclusion

The preparation of a new substrate for SERS applications is usually accompanied by a comparison of its performance in relation to well-established SERS substrates like colloidal AuNS. Its quality as a good SERS substrate relies on the comparison among the SERS-EF values. In the present work, the lowest SERS-EF has been measured for AuNS (in the order of 10^3) under the same conditions as the ones used in the SERS-EF evaluation for different static substrates (millimolar concentration of 4MPy). The low SERS-EF measured for AuNS is associated with the generation of aggregates with many nanoparticles due to the high concentration of 4MPy causing the plasmon resonance to be far from the laser excitation wavelength. However, even when additional experiments under low concentrations have been performed (nanomolar concentration of 4MPy), aiming at forming the smallest possible aggregates and verifying whether the low SERS-EF for AuNS has been caused by the high concentration conditions, a larger SERS-EF has been obtained under 785 nm excitation than under 633 nm. Therefore, it can be confirmed that in spite of lower concentrations, the employed probe is still capable of promoting the aggregation of AuNS.

The present work shows that this type of comparison may not be a good performance analysis criterion in the case of a dynamic substrate such as AuNS. The reason for this originates from the dynamic nature of the AuNS substrate, *i.e.*, the simple addition of the probe molecule (the smallest possible concentration) may promote striking changes in the aggregation state of the particles in solution and therefore, on the substrate's optical and near field properties. The variation after the addition of 4MPy is due to the strong chemical interaction with AuNS, a situation that favours the exchange of the stabilizing citrate layers and reduces the colloidal stability, allowing for the aggregation to happen.

The experimental SEM images and SERS in the nanomolar range along with the GMT results have indicated a condition that enables a reasonable comparison between AuNT and AuNS substrates. If the latter were constituted mostly of dimers and trimers, the plasmon resonance would be measured in the same regions as the AuNT substrates and the SERS-EF would be set by the plasmonic properties of the aggregates. This condition is not easily achieved experimentally. The commonly used AuNS suspensions do not fulfil this condition.

The main purpose of the present work is to show that by keeping the same experimental conditions for the two experiments (the static and dynamic substrates), the addition of the probe-molecule will induce a striking aggregation of the particles for the dynamic substrates and therefore, a striking change in that substrate's optical properties and SERS performance.

Furthermore, a proper comparison among SERS substrates may only be made if the optical properties, translated by the localized surface plasmon resonance wavelength, are the same. This situation is not simple to control experimentally in the case of a dynamic substrate such as AuNS. This difficulty makes the comparison of SERS-EF values for static and dynamic SERS substrates meaningless.

Acknowledgements

Notes and References

1 K. Chang and T. E. Furtak, *Surface Enhanced Raman Scattering*, Plenum Press, New York, 1982.
2 R. Aroca, *Surface-Enhanced Vibrational Spectroscopy*, John Wiley & Sons, New York, 2006.
3 E. C. Le Ru and P. G. Etchegoin, *Principles of Surface-Enhanced Raman Spectroscopy: and related plasmonic effects*, Elsevier, Amsterdam, 2009.
4 P. L. Stiles, J. A. Dieringer, N. C. Shah and R. R. Van Duyne, *Annu. Rev. Anal. Chem.*, 2008, **1**, 601–626.
5 E. C. Le Ru, E. Blackie, M. Meyer and P. G. Etchegoin, *J. Phys. Chem. C*, 2007, **111**, 13794–13803.
6 M. K. Fan, G. F. S. Andrade and A. G. Brolo, *Anal. Chim. Acta*, 2011, **693**, 7–25.
7 R. Gordon, D. Sinton, K. L. Kavanagh and A. G. Brolo, *Acc. Chem. Res.*, 2008, **41**, 1049–1057.
8 J. P. Camden, J. A. Dieringer, J. Zhao and R. P. Van Duyne, *Acc. Chem. Res.*, 2008, **41**, 1653–1661.
9 D. C. Rodrigues, G. F. Souza Andrade and M. L. Arruda Temperini, *Phys. Chem. Chem. Phys.*, 2013, **15**, 1169–1176.
10 P. H. B. Aoki, E. G. E. Carreon, D. Volpati, M. H. Shimabukuro, C. J. L. Constantino, R. F. Aroca, O. N. Oliveira and F. V. Paulovich, *Appl. Spectrosc.*, 2013, **67**, 563–569.
11 D. Y. Wu, J. F. Li, B. Ren and Z. Q. Tian, *Chem. Soc. Rev.*, 2008, **37**, 1025–1041.
12 R. F. Aroca, R. A. Alvarez-Puebla, N. Pieczonka, S. Sanchez-Cortez and J. V. Garcia-Ramos, *Adv. Colloid Interface Sci.*, 2005, **116**, 45–61.
13 J. F. Li, Y. F. Huang, Y. Ding, Z. L. Yang, S. B. Li, X. S. Zhou, F. R. Fan, W. Zhang, Z. Y. Zhou, D. Y. Wu, B. Ren, Z. L. Wang and Z. Q. Tian, *Nature*, 2010, **464**, 392–395.
14 D. P. dos Santos, G. F. S. Andrade, M. L. A. Temperini and A. G. Brolo, *J. Phys. Chem. C*, 2009, **113**, 17737–17744.
15 D. P. dos Santos, G. F. S. Andrade, A. G. Brolo and M. L. A. Temperini, *Chem. Commun.*, 2011, **47**, 7158–7160.
16 D. P. dos Santos, M. L. A. Temperini and A. G. Brolo, *J. Am. Chem. Soc.*, 2012, **134**, 13492–13500.
17 E. C. Le Ru and P. G. Etchegoin, in *Annu. Rev. Phys. Chem.*, ed. M. A. Johnson and T. J. Martinez, 2012, vol. 63, pp. 65–87.
18 J. C. S. Costa, R. A. Ando, A. C. Sant'Ana, L. M. Rossi, P. S. Santos, M. L. A. Temperini and P. Corio, *Phys. Chem. Chem. Phys.*, 2009, **11**, 7491–7498.
19 X. X. Han, B. Zhao and Y. Ozaki, *Anal. Bioanal. Chem.*, 2009, **394**, 1719–1727.
20 X. Shi, J. Ma, R. Zheng, C. Wang and H.-D. Kronfeldt, *J. Raman Spectrosc.*, 2012, **43**, 1354–1359.
21 S. E. J. Bell and N. M. S. Sirimuthu, *Chem. Soc. Rev.*, 2008, **37**, 1012–1024.
22 C. M. S. Izumi, G. F. S. Andrade and M. L. A. Temperini, *J. Phys. Chem. B*, 2008, **112**, 16334–16340.
23 L. Guerrini, J. V. Garcia-Ramos, C. Domingo and S. Sanchez-Cortes, *Anal. Chem.*, 2009, **81**, 1418–1425.
24 M. L. de Souza and P. Corio, *Appl. Catal., B*, 2013, **136–137**, 325–333.
25 M. L. de Souza, D. C. Tristao and P. Corio, *RSC Adv.*, 2014, **4**, 23351–23358.
26 W. B. Cai, B. Ren, X. Q. Li, C. X. She, F. M. Liu, X. W. Cai and Z. Q. Tian, *Surf. Sci.*, 1998, **406**, 9–22.
27 G. Frens, *Nature (London), Phys. Sci.*, 1973, **241**, 20–22.
28 H. E. Toma, V. M. Zamarion, S. H. Toma and K. Araki, *J. Braz. Chem. Soc.*, 2010, **21**, 1158–1176.
29 Z.-B. Lin, J.-H. Tian, B.-G. Xie, Y.-A. Tang, J.-J. Sun, G.-N. Chen, B. Ren, B.-W. Mao and Z.-Q. Tian, *J. Phys. Chem. C*, 2009, **113**, 9224–9229.
30 Z. Q. Tian, B. Ren and D. Y. Wu, *J. Phys. Chem. B*, 2002, **106**, 9463–9483.
31 S. Trasatti and O. A. Petrii, *Pure Appl. Chem.*, 1991, **63**, 711–734.
32 M. Ringler, A. Schwemer, M. Wunderlich, A. Nichtl, K. Kuerzinger, T. A. Klar and J. Feldmann, *Phys. Rev. Lett.*, 2008, **100**, 203002.
33 Y. L. Xu, *Appl. Opt.*, 1997, **36**, 9496–9508.
34 Y. L. Xu, *Appl. Opt.*, 1998, **37**, 6494.
35 Y. L. Xu, *Phys. Lett. A*, 1998, **249**, 30–36.
36 P. B. Johnson and R. W. Christy, *Phys. Rev. B: Condens. Matter Mater. Phys.*, 1972, **6**, 4370–4379.
37 M. Moskovits and D. P. Dilella, *J. Chem. Phys.*, 1980, **73**, 6068–6075.
38 L. J. Wan, Y. Hara, H. Noda and M. Osawa, *J. Phys. Chem. B*, 1998, **102**, 5943–5946.
39 T. Sawaguchi, F. Mizutani, S. Yoshimoto and I. Taniguchi, *Electrochim. Acta*, 2000, **45**, 2861–2867.
40 L. Rodriguez-Lorenzo, R. A. Alvarez-Puebla, I. Pastoriza-Santos, S. Mazzucco, O. Stephan, M. Kociak, L. M. Liz-Marzan and F. J. G. de Abajo, *J. Am. Chem. Soc.*, 2009, **131**, 4616–4618.
41 J. C. Fraire, L. A. Pérez and E. A. Coronado, *J. Phys. Chem. C*, 2013, **117**, 23090–23107.
42 J. Hu, B. Zhao, W. Xu, Y. Fan, B. Li and Y. Ozaki, *J. Phys. Chem. B*, 2002, **106**, 6500–6506.
43 B. L. Darby and E. C. Le Ru, *J. Am. Chem. Soc.*, 2014, **136**, 10965–10973.